1
2

Experimental and numerical identification of corrosion degradation of ageing structural components

3   Beata Zima[a], Krzysztof Woloszyk[a], Yordan Garbatov[b, 1]

4   [a] Institute of Ocean Engineering and Ship Technology, Gdansk University of Technology,
5   G. Narutowicza 11/12 st., 80-233 Gdansk, Poland
6   [b] Centre for Marine Technology and Ocean Engineering (CENTEC), Instituto Superior Técnico,
7   Universidade de Lisboa, Avenida Rovisco Pais 1049-001 Lisboa, Portugal

8   **Abstract**

9   The study presents experimental and numerical identification of corrosion degradation of thin-
10   walled structural components employing guided wave propagation. The steel structural
11   components are subjected to through-thickness varying corrosion degradation levels. The
12   developed approach using the non-destructive guided wave-propagation quantifies the
13   equivalent average corrosion degradation level exploring a limited number of transducers. A
14   group velocity dispersion curve reconstruction has been used to determine the corrosion-
15   induced plate thickness reduction. Two case studies are used to examine experimentally the
16   newly developed approach. In the first one, the dispersion curve and the assessment of the
17   corrosion thickness reduction have been made using wave signals of various excitation
18   frequencies. In the second one, the analysis has been conducted only for two wave propagation
19   signals and one excitation frequency which allowed for reconstructing the dispersion curve in
20   a limited frequency range. In both case studies, a good agreement between the natural and
21   estimated corrosion degradation levels was observed. The present study develops a signal
22   processing methodology, which can be used in the SHM systems, where several aspects still
23   need to be further investigated before it can be applied in large size and complex geometry of
24   ship hull structures.

25   **Keywords:**

26   corrosion degradation; steel plates; ship structures; NDT; ultrasonic waves

27   **1   Introduction**

28   Ships and offshore structures are operating in a highly corrosive environment. The
29   excessive corrosion degradation may lead to catastrophic consequences, e.g., exceedance of the

---

[1] Corresponding author e-mail: yordan.garbatov@tecnico.ulisboa.pt; Telf (351) 21 841 7907

30 ultimate strength of ship structural components (Woloszyk et al., 2018) and entire ship hull

31 (Parunov et al., 2007). According to Zayed et al. (Zayed et al., 2018), even up to 90% of ship

32 hull damages are primarily or indirectly caused by corrosion. An example of tanker ship loss,

33 mainly driven by excessive corrosion degradation, breaking the ship's hull in two parts, is the

34 tanker Prestige in 2002 (Flashback history: Tanker Prestige sinking (Video), 2015).

35   There are regular surveys of the entire ship to avoid severe degradation, where the

36 thickness of structural components is measured using an ultrasonic thickness gauge. This

37 method has various advantages, i.e., the equipment is portable, and the usage is user-friendly.

38 However, it provides information about thickness in one point of any particular measurement.

39 Thus, numerous thickness measurements must be done to correctly map the distribution of

40 thickness corrosion diminutions within larger structures like ship hulls.

41   Cegla and Gajdacsi (Cegla and Gajdacsi, 2016) found that irregularities in corroded

42 surfaces disturb the ultrasonic measurements and usually overestimate the corroded plate

43 thickness value. Similar observations have been found in (Woloszyk et al., 2021). Zayed et al.

44 (Zayed et al., 2008) analysed the factors that may disturb the ultrasonic measurements, e.g.

45 lighting, cleanliness and accessibility to the inspected area. Additionally, there is always a

46 probability that some deteriorated structural components are omitted during the inspections.

47 Such a possibility may be seen in a more difficult area for inspection as double bottom or closed

48 spaces.

49   To reflect some problems faced with using the non-destructive measuring techniques,

50 some new approaches were developed, especially based on guided waves, which were proved

51 to be very useful in diagnostics of both localized damages (Cao et al., 2021; Wandowski et al.,

52 2011; Zima, 2021), as well as surface damages (Ding et al., 2021; Hu et al., 2022; Zima and

53 Rucka, 2017). The guided wave propagation seems to define the corrosion degradation level

54 around the structural components effectively. The most advantageous feature of the guided

55 wave propagation approach is mapping a larger area of the thickness of structural components.

56 Moreover, high-frequency wave-based methods are generally insensitive to applied loads and

57 low-stress levels (the differences in wave velocities are negligible), which significantly

58 facilities the analysis and results interpretation (Li et al., 2021).

59   Ervin and Reis (Ervin and Reis, 2008) tested the guided waves' low and high-frequency

60 ranges to monitor the reinforced bar's corrosion degradation in mortar specimens. Ervin et al.

61 (Ervin et al., 2009) used longitudinal ultrasonic waves of high frequencies to monitor the

62 reinforced mortar specimens undergoing accelerated uniform and localised corrosion.

63   Two ultrasonic techniques of pulse transmission and pulse-echo were used to monitor the

64   healthy and damaged bar by Sharma and Mukherje (Sharma and Mukherjee, 2010). Fractal

65   analysis of guided ultrasonic waves for evaluating the corrosion degradation level in post-

66   tensioned systems was proposed by Moustafa et al. (Moustafa et al., 2014). Farhidzadeh and

67   Salamone (Farhidzadeh and Salamone, 2015) used dispersion curves, continuous wavelet

68   transform, and wave velocity measurement to quantify the corrosion damage of multiwire

69   prestressing steel strands.

70   In all reported cases, the corrosion degradation was accelerated by applying the direct

71   current. The level of corrosion degradation (mass loss) was linearly dependent on corrosion

72   current and time elapsed. The corrosion degradation assessment was based on the analysis of

73   the dispersion curves. Because the shape of dispersion curves mainly depends on the geometric

74   parameters, monitoring the trace changes efficiently assessed the corrosion degradation level.

75   Recently the methods of dispersion curve reconstruction have been extensively studied.

76   However, the dispersion curve reconstruction demands multiple measurements along the

77   relatively short propagation path, which would be inefficient in a large-scale structure like

78   offshore platforms or ships (Draudviliene et al., 2021). Finally, there are almost no studies

79   regarding guided wave propagation to identify the corrosion degradation of thin-walled

80   structures subjected to environmental corrosion. Most of the studies were related to localised

81   pitting corrosion (Ciampa et al., 2015; Ding et al., 2021; Howard and Cegla, 2017; Hua et al.,

82   2020; Tian et al., 2021). The corrosion degradation observed in ship structures is mainly general

83   (Panayotova and Garbatov, 2010), although pitting one is quite common too. General corrosion

84   is observed, e.g., in cargo holds as well as in ballast tanks.

85   Recently, the study aimed at a corrosion assessment using the guided ultrasonic waves

86   (Zima et al., 2022), contained a detailed description of a methodology based on the phase

87   velocity and convex optimization. The study performed here is the next step aimed at procedure

88   simplification and reducing the extent of the sensors network, as well as the collected data in

89   the future SHM systems. Previously employed phase velocity was determined using spectral

90   decomposition and the zero-cross method. Because of the dispersive nature of guided waves

91   and spreading the wave packet, the unambiguous identification of corresponding roots may be

92   associated with impediments to interpretation. Moreover, it was proved that usually the phase

93   velocity is overestimated which leads to underestimation of corrosion degradation level [20].

94   Therefore, in the following study, the approach based on dispersion curve reconstruction has

95   been modified and we have used the Hilbert transform and group velocity curve to assess the

96   degradation level of thin-walled ship structures. Such modifications allow for simplification of

the signal processing procedure. The newly developed approach's main advantage is that only two adjacent wave propagation signals are needed in the identification process. The limited number of essential signals processed within the algorithm is extremely important from the point of view of the further development of the diagnostics systems and data communication. The smaller number of signals requires fewer measurements which in turn means a smaller size of memory and the whole size of the potential devices. Additionally, the smaller size of the device and a limited number of excitations and registrations entail longer battery life and lower costs of equipment maintenance. Although the presented algorithm is only the first step in the development of the diagnostics methods for ship structural monitoring and its requirement improvements which are faithfully discussed in the paper, the small amount of necessary data is one of its most significant advantages.

The corrosion degradation level of a significant area may be assessed, which makes the newly developed approach far more effective than the standard one of the ultrasonic thickness measurement or wave tomography. The analysed corroded thin-walled structural components were initially corroded employing an originally designed corrosion deterioration set-up. The corrosion degradation process was in line with in-situ environmental degradation. The designed corrosion deterioration set-up has a significant advantage over the efficient DC-induced corrosion degradation and leads to more realistic surface characteristics (Xiao et al., 2020; Yuan et al., 2007), but is still very different from the real one.

Based on the obtained reconstructed dispersion curves the corrosion degradation level has been assessed. To analyse the effectiveness and accuracy of state assessment of the specimen, the analysis stage has been divided into two stages. Within the first stage, five different frequencies were used in the study and the curves have been reconstructed in the wide frequency range. At the second stage, the curve was traced only for a narrow frequency range reconstructed after one excitation. In both cases, the progress of corrosion degradation affected the shape of the curves. The results collected within both stages were compared with the actual one determined by mass calculation. The agreement between the results suggests the potential of the novel method in corrosion degradation monitoring. The article discusses both advantages and disadvantages of the proposed method.

126   **2   Guided waves propagation in thin-walled structures**

127   *2.1   Theoretical background*

128   The guided waves in plates are generated due to the interaction of compressive and shear
129   waves propagating in elastic, homogeneous, isotropic medium bounded with two equidistant
130   surfaces. Horace Lamb foresaw their existence (Lamb, 1917) and derived dispersion equations
131   relating to the propagation velocity and the number of possible wave modes with an excitation
132   frequency. In general, the Lamb waves can exist as symmetric and antisymmetric. They are
133   high dispersive, and their propagation velocity depends on the frequency and plate thickness
134   product. Two equations describe the dispersive characteristics of both types:

135
$$\frac{\tan(qd)}{\tan(pd)} = -\frac{\left(k^2 - q^2\right)^2}{4k^2 pq}, \tag{1a}$$

136
$$\frac{\tan(qd)}{\tan(pd)} = -\frac{4k^2 pq}{\left(k^2 - q^2\right)^2} \tag{1b}$$

137   where d is the plate thickness and the parameters p and q depend on wavenumber k, angular
138   frequency ω, longitudinal wave velocity (c_L) or shear wave velocity (c_T) in the infinite
139   medium. The velocities of guided and bulk waves depend also on the material parameters of
140   the considered medium. Eqn 1a is associated with symmetric particle motion about the
141   midplane, while Eqn 1b describes the antisymmetric particle motion caused by wave
142   propagation. The number of possible solutions fulfilling the Eqn (1) is infinite, and in general,
143   the roots may be complex. However, the real roots are associated with propagating waves, while
144   imaginary roots corresponding to evanescent waves will not be considered in further analysis.
145   The solution of the dispersion equation is presented in the form of dispersion curves. At least
146   one symmetric mode (S) resembling axial waves and one antisymmetric mode (A) resembling
147   flexural wave exists for each frequency. The number of possible curves associated with any
148   particular wave mode increases with the increase of the considered frequency range. The
149   exemplary dispersion curves traced for a steel plate are presented in Figure 1.
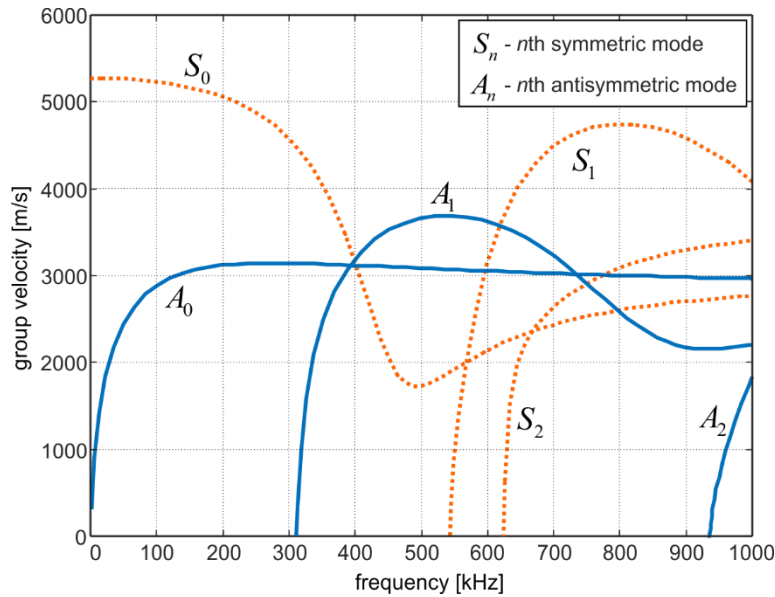
Figure 1 Dispersion curves for a steel plate with a thickness of 5 mm, elastic modulus E = 198 GPa, v = 0.3 and density 7,850 kg/m³

It has to be pointed out that the Lamb theory is valid only for plates with constant thickness, and their material fulfils the conditions of elasticity, homogeneity, and isotropy. Meanwhile, the corroded specimens are usually covered with corrosion products varying in mechanical properties from the undamaged core. In general, the additional layers require different wave theories, but in the following study, the corrosion products were removed before the investigation to assess the damage degradation level. This research will verify the correctness of the assumption about the constant thickness.

2.2 Signal processing procedure

As mentioned, the shape of dispersion curves depends on the material and geometric parameters of the considered plate. The proposed approach for a corrosion level assessment assumes that corrosion degradation influences the thickness of the plate. At the same time, the elastic modulus, density, and Poisson's ratio are considered to remain unaffected. In consequence, the shape of the dispersion curve depends on the corrosion deterioration level. In general, the assumption about the constant material parameters is not valid for cases of corroded structures and will be verified in this study. However, the plate thickness is the most influential factor, and its variation affects the wave velocity the most. Figure 2 presents the dispersion curve associated with the first antisymmetric Lamb mode in the frequency range (0-500 kHz) for steel plates with varying thicknesses. For some frequencies, the degree in the group propagation velocities is significant (i.e., 100 kHz). In contrast, for some frequencies, the curves

6

172 coincide with each other, which indicates that the corrosion degradation (plate thickness

173 reduction) does not impact the wave propagation (i.e., 400-500 kHz).

174
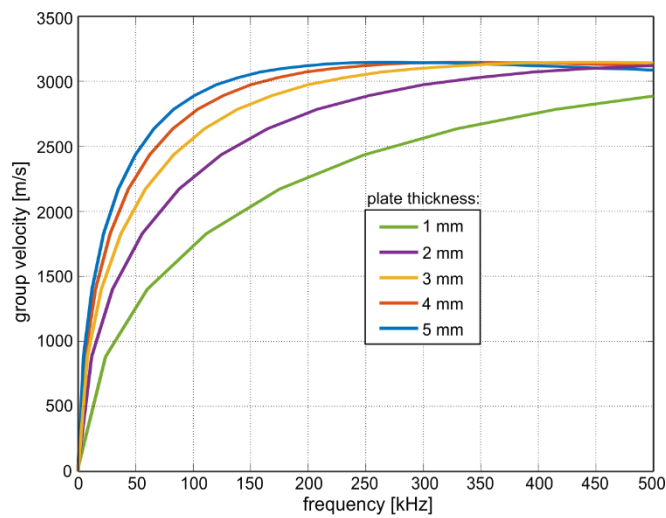
176 Figure 2 Dispersion curve associated with the first antisymmetric Lamb mode for plates with a varying thickness

177

178   Moreover, the corrosion degradation impact depends on the initial parameters of the

179 uncorroded plate. One-millimetre thickness reduction in a plate with an initial thickness of 5

180 mm results in an insignificant change in the dispersion curve shape. In contrast, in the case of

181 thinner plates, the difference is noticeable. There is no explicitly given relationship between the

182 frequency, propagation velocity, and thickness reduction. However, for every thickness,

183 frequencies of corrosion damage can be identified. The newly developed approach here aims to

184 reconstruct the dispersion curve representing group velocity, enabling a better estimation of the

185 average plate thickness during corrosion degradation.

186   The corrosion degradation level identification is based on measuring at least two signals

187 by the transducers attached at two distinct positions. The distance between the actuator and

188 sensors should be established by taking into account the dispersive nature of guided waves,

189 signal attenuation, the energy of the input wave, and the size of the area, which is monitored.

190 The shorter distance results in a greater signal-to-noise ratio (SNR), which facilities the

191 interpretation of the results. The longer distance allows for assessing a greater area of the tested

192 structure.

193   The algorithm presented here aimed at the reconstruction of dispersion curves using

194 adjacent signals has been also analysed and utilized by other researchers (Draudviliene et al.,

195 2021; Zima et al., 2022). The main development is its modification for group velocity extraction

196 and employment in the corrosion degradation assessment. For clarity, a brief description of the

197 following steps is presented here.

7

198   In the first step of the developed approach, the guided Lamb waves are excited by an

199 actuator triggering a narrowband burst. In this study, the five-cycle sinusoid modulated by the

200 Hann window is used (Lyons, 2011):

$$p(t) = \begin{cases} p_0 \sin(2\pi f t) \cdot w(t) & t \in [0, T_w] \\ 0 & t \geq T_w \end{cases}, \tag{2}$$

202 where f is the excitation frequency, p_0 denotes the excitation amplitude, and T_w is the modulating

203 window length. The modulation window is described by a function:

$$w(t) = 0.5 \left(1 - \cos\left(\frac{2\pi f t}{n_w} \right) \right), \quad t \in [0, T_w], \tag{3}$$

205   Next, the incident waves captured by sensors are identified and extracted from the

206 adjacent signals (Figure 3, stage II). The reflections from the edges or other obstacles registered

207 further in the signal are not considered, significantly simplifying the analysis, which is one of

208 the most important advantages of this approach, especially in the context of the further research

209 dedicated to diagnostics of large and complex structures. The trigonometric representations of

210 the incident waves are calculated using the Fourier integral and the frequency response

211 amplitude (Figure 3, stage III). The spectrum is normalised as the maximum value equals 1.0

212 in each case (Figure 3, stage IV). Based on the frequency ranges of the obtained spectra, the

213 frequency limits f_L and f_H are established. In general, the spectrum vanishes above the upper-

214 frequency limit f_H and below the lower frequency limit f_L (Figure 3, stage V). Regardless of

215 the spectra' differences for signals registered during the same measurement, the frequency limits

216 are the same. Next, the frequency spectra $S(f)$ are filtered by using n bandpass filters defined

217 as a Gaussian magnitude function:

$$U_k(f) = S(f) B_k(f) = S(f) e^{4\ln(0.5)\left(\frac{f - f_L - (k-1)df}{\Delta B}\right)^2}, \tag{4}$$

219 and $k = 1, 2, \ldots n$. According to recommendations formulated by He (Ping He, 1998), the number

220 of filters n depends on the bandwidth parameter ΔB, which defines the frequency range limited

221 by the single filter:

$$n > 1 + \frac{f_H - f_L}{\Delta B}, \tag{5}$$

223   Here, the bandwidth parameter ΔB was determined based on the normalised Fourier

224 frequency spectrum. Its value was established based on the spectrum width for the normalised

225 amplitude corresponding to the -3dB value. In the next stage, the signal is synthesised from the

226 basic trigonometric functions by using the inverse Fourier transform (Figure 3, stage VI).

227 Finally, the time of flight was determined by the envelope method. The envelope of the signal
228 was calculated using the Hilbert transform (Figure 3, stage VII and VIII). The time of flight
229 was computed using the cross-correlation method and was defined as the peak-to-peak value.
230 The group velocity of Lamb waves was calculated as the distance x divided by the time of the
231 flight. The shape of the dispersion curve was reconstructed by plotting the set of frequencies
232 and corresponding group velocities (Figure 3, stage IX). Employing the group velocity instead
233 of the phase velocity as a quality indicator significantly facilities the robustness of the
234 developed procedure.

I. experimental measurements   II. incident wave identification   III. Fourier transform

IV. spectrum normalization

V. spectrum filtering   VI. inverse Fourier transform

VII. Hilbert transform

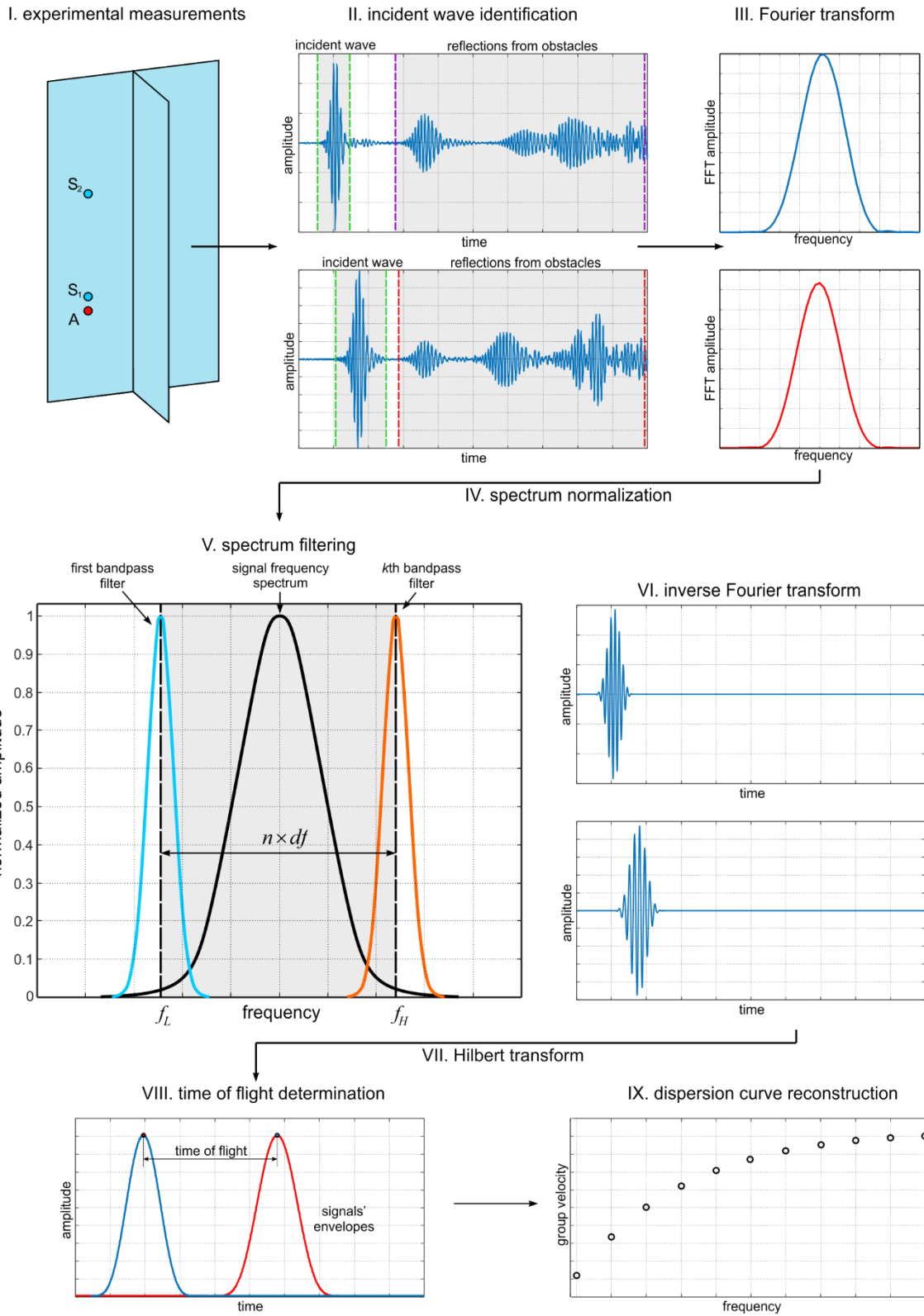VIII. time of flight determination   IX. dispersion curve reconstruction

Figure 3 Signal processing procedure

The frequency range within the shape of the dispersion curve can be reconstructed based on the excitation frequency, the width of the signal spectrum, and spectra frequency limits f_L and f_H. In general, the segments of dispersion curves obtained for various frequencies may

240 overlap (Figure 4a). In such a case, the procedure has been extended by an additional step, and
241 the group velocity was averaged within the common frequency region (Figure 4b).
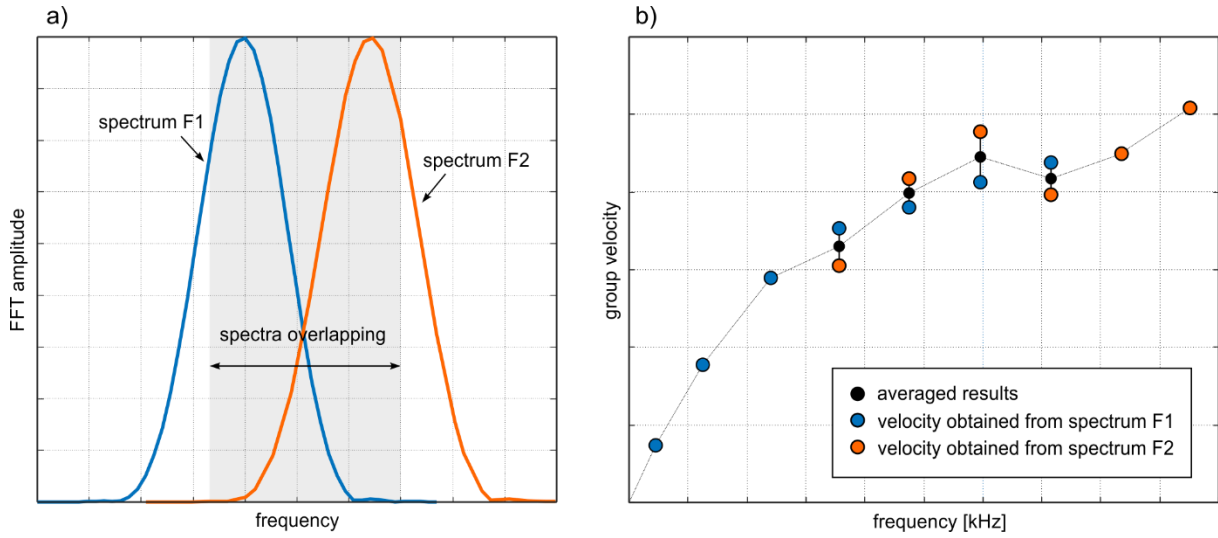
Figure 4 Processing of experimental data: a) spectra overlapping and b) averaging of group velocity determined in a common frequency range of both spectra

2.3 Identification of corrosion degradation level

246 To estimate the thickness reduction based on the reconstructed dispersion curve, first, the
247 dependence for the first antisymmetric Lamb mode A_0 was calculated for the pre-established
248 plate thickness d. Then, the dispersion curve determined numerically based on the analytical
249 equation was considered as the sets of n pairs of numbers:

$$C_{gr}^T(d) = \left\{ \left(\Delta f, c_{gr}^T(\Delta f) \right), \left(2\Delta f, c_{gr}^T(2\Delta f) \right), ..., \left(n\Delta f, c_{gr}^T(n\Delta c_{gr}) \right) \right\} = \left\{ \left(\Delta f, c_{gr}^{T,1} \right), \left(2\Delta f, c_{gr}^{T,2} \right), ..., \left(n\Delta f, c_{gr}^{T,n} \right) \right\}$$

251 The second set of data was obtained from the experimental analysis:

$$C_{gr}^E = \left\{ \left(\Delta f, c_{gr}^E(\Delta f) \right), \left(2\Delta f, c_{gr}^E(2\Delta f) \right), ..., \left(n\Delta f, c_{gr}^E(n\Delta c_{gr}) \right) \right\} = \left\{ \left(\Delta f, c_{gr}^{E,1} \right), \left(2\Delta f, c_{gr}^{E,2} \right), ..., \left(n\Delta f, c_{gr}^{E,n} \right) \right\}$$

253 Next, the value of the following function has been calculated:

$$Y(d) = \frac{1}{n} \sum_{i=1}^{n} \left(y_i(d) \right)^2 = \frac{1}{n} \sum_{i=1}^{n} \left(c_{gr}^{T,i}(d) - c_{gr}^{E,i} \right)^2 \tag{10}$$

255 The calculations were performed for a varying plate thickness. The function $Y(d)$ reached
256 the minimum value for the best matching of numerical and experimental dispersion curves
257 (Figure 5).

11
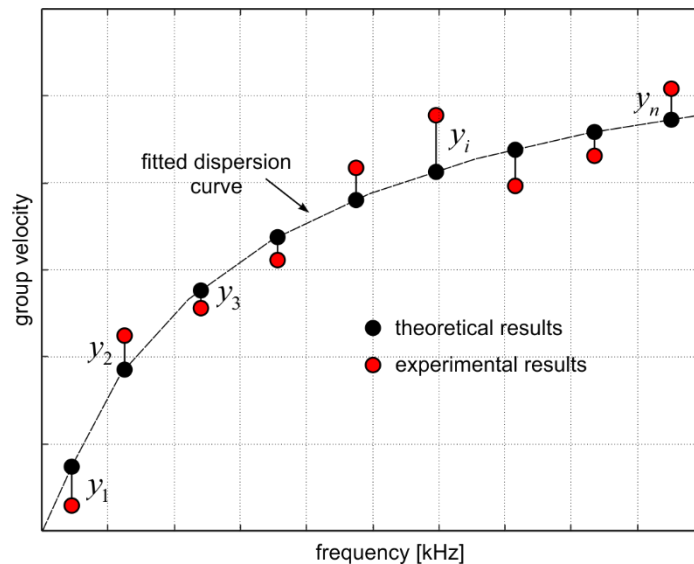
Figure 5 Matching of experimental and analytical results

In general, one can say that a similar effect in the form of a dispersion curve can be easily obtained using different excitation types i.e., broadband pulse excitation providing triggering multiple frequencies at the same time. This approach has been widely tested in corrosion assessment applications and its effectiveness in dispersion curve reconstruction based on Short Time Fourier Transform has been demonstrated. However, the broadband pulse excitation has several disadvantages which caused to decide to employ narrowband excitation. First of all, simultaneous excitation of several frequencies is associated with multiple wave mode excitation and further conversions. In the case of the specimens with more complex geometry and several modes varying in carrier frequency and velocity, it would be difficult to extract the part of the signal which should be processed. The second important reason is the possible application in real monitoring systems. Narrowband excitation associated usually with one single wave mode is much more effective in the detection of localized damage like corrosion pits or cracks. It is particularly important as long these two types of corrosion damage can occur simultaneously. Despite the fact this paper considers only general corrosion, the application of narrowband excitation potentially allows for both general corrosion degradation assessment (Zima et al., 2022), as well as the detection and localization of other damage types (Zima, 2021).

3   Experimental study

The experimental analysis of a stiffened steel plate was conducted, which is considered a primary structural component of the ship hull girder (Figure 6). The analysed stiffened plate was of 5 mm thickness, and its geometry is presented in Figure 6. The mechanical properties were determined via tensile tests of coupon specimens according to ISO standard (ISO, 2009).

282 The mean value from seven samples was estimated for the elastic modulus of 198 GPa and
283 yield stress of 272.3 MPa.
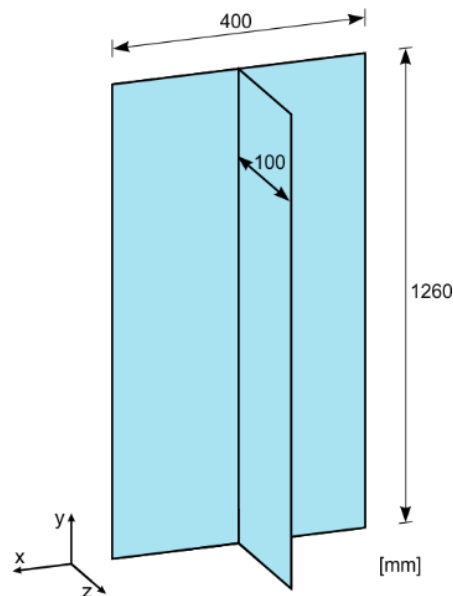
Figure 6. Stiffened plate geometry.

3.1 Corrosion degradation

287   The corrosion testing set-up was presented in (Woloszyk et al., 2021), together with the
288 analysis of the generated corrosion degradation. The accelerated marine immersed corrosion
289 degradation was generated by controlling the most important natural factors without applying
290 DC. The specimens were placed in a 900-litre tank made from glass-reinforced plastic. The
291 controlled environmental factors were the salinity (35 ppm), water circulation (induced by the
292 circulation pumps), temperature (approx. 35 °C, increased by heaters), and dissolved oxygen
293 content (augmented by the aeration pump over the limit of fully saturated conditions). The
294 periodical measurements of the stiffened plate specimen's mass were carried out using the scale
295 with an accuracy of 2 g. Based on that, the propagation of each specimen's mean value corrosion
296 diminution with the time was determined. The mean corrosion rate obtained for 5 mm
297 specimens was equal to 0.774 mm/year, and the total duration of the corrosion tests was 428
298 days. In comparison to long-lasting experiments in natural seawater conditions, accelerated
299 testing was a very efficient method. In real ship structures, the mean corrosion rate of the
300 structures does not exceed the level of 0.1 mm/year (Melchers, 2008).
301   Three specimens of an initially 5 mm thickness were corroded, and three different
302 degradation levels (calculated as the percentage loss of the initial mass of the specimen) were
303 generated namely: 7%, 14% and 21%, by pulling the samples out of the water at different times.
304 Although plate surfaces of different initial thicknesses were also corroded, the 5 mm plates

13

305 were chosen for validation of the new methodology. The thickness variability increased with
306 the corrosion degradation level growth. Figure 7a shows the most severely corroded specimen,
307 while Figure 7b presents the surfaces of any particular specimens.
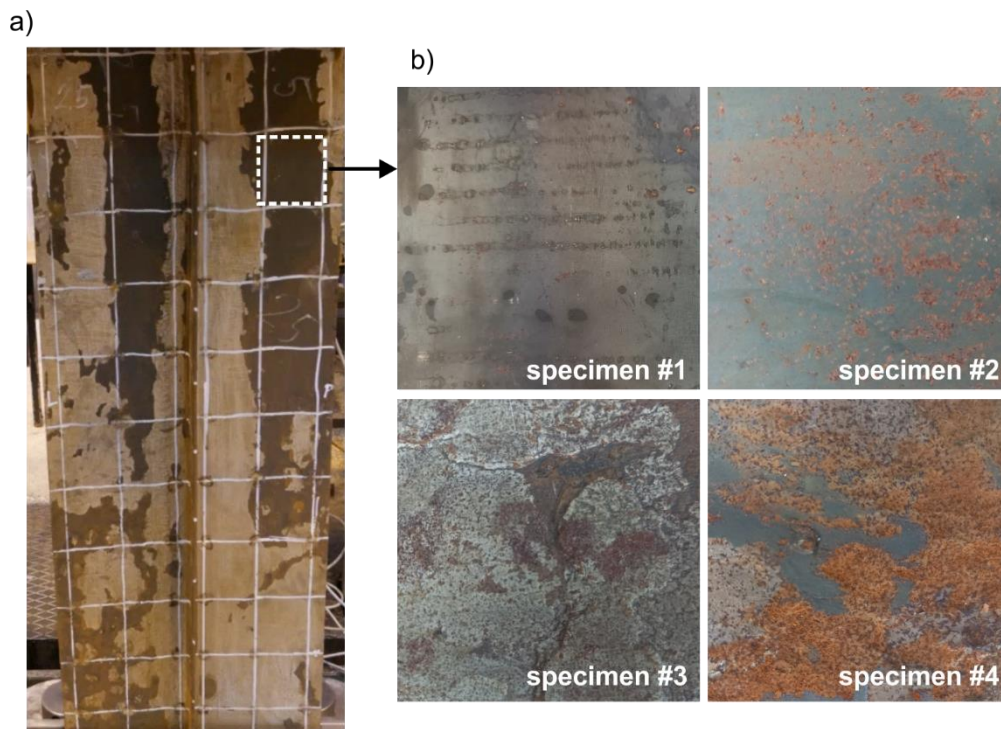
309   Figure 7 Corroded specimens: a) specimen with 21 % degradation level and b) surfaces of corroded specimens

311 It must be mentioned here that between environmental accelerated corrosion and the actual
312 corrosion process some differences may occur, especially concerning the internal
313 microstructure of the corroded element. However, the current study is mainly focused on the
314 guided wave-based diagnostics method and recent studies (Zima, 2022) proved that the wave
315 propagation velocity, as well as the time course of the signals, are dependent only on specimen
316 thickness distribution. It means that two specimens varying in geometry but with the same
317 thickness distribution will result in the same velocity and shape of the incident wave. Thus, the
318 speed of the corrosion process has no direct influence on wave propagation signals but the
319 resulting thickness variability and differences in specimen geometry may affect signal
320 characteristics.

321 *3.2   Guided wave propagation*

322   The excitation and measurements of elastic waves were carried out by an experimental
323 set-up comprised of an oscilloscope, function generator and piezoelectric transducers Noliac
324 NAC2024. To improve the signal-to-noise ratio, the receiver was connected to the high voltage

14

325   amplifier ThorLab. The Lamb wave excitation was realised as a wave packet consisting of a

326   five-cycle sine modulated by a Hann window. The carrier frequency was from 50 to 250 kHz

327   with a step of 50 kHz (Figure 8a). The proposed algorithm has been tested for a low-frequency

328   range to avoid the excitation of the higher-order modes. The sampling frequency was 500 MHz,

329   and the input voltage was 20 V. To minimise the influence of electrical noises in the amplifier,

330   each signal was averaged 1024 times. The perpendicular excitation is associated with triggering

331   the propagation of flexural waves. Despite that, the presented reasoning is also valid for

332   symmetric modes, from practical reasons it is much easier to attach the transducer at the plate

333   surface rather than at the free edge. Therefore, further analysis concerns the antisymmetric

334   Lamb modes defined by Eq. (1b).

335   The first signal was captured at 10 mm from the excitation source, while the second was

336   310 mm. The distance x between sensors was 300 mm (Figure 8c).
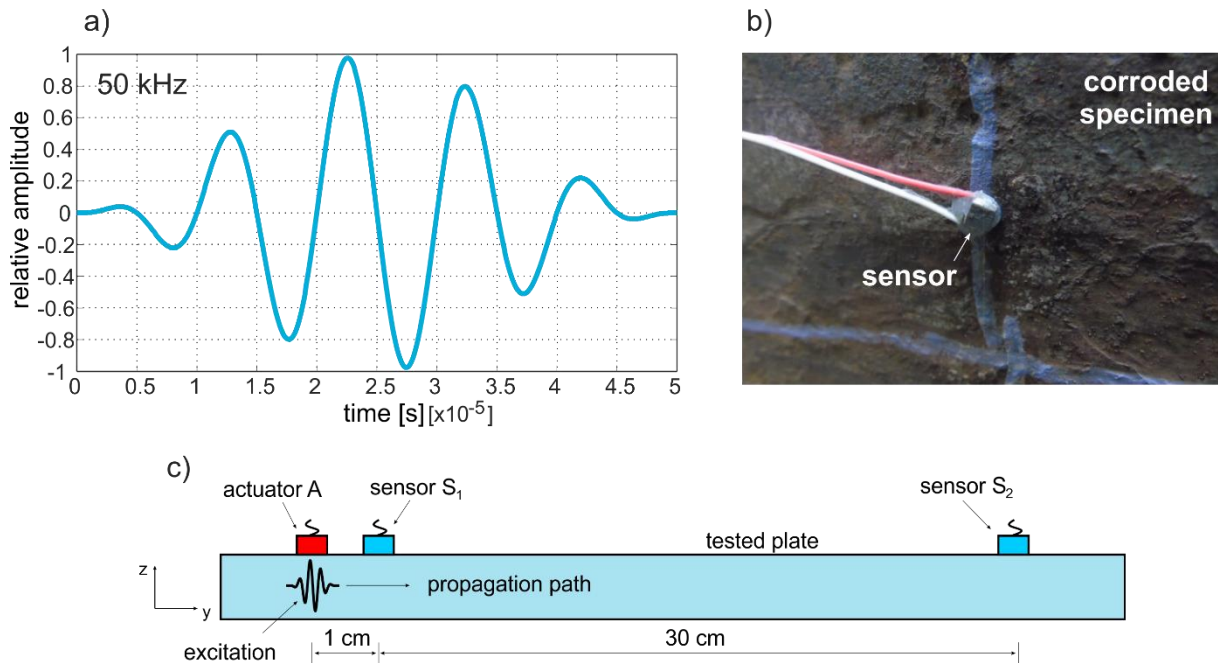
337

338   Figure 8 Experimental tests: a) excitation functions and b) sensor attached at the corroded plate surface, c)
339   configuration of the transducers

340   The waves were propagated along the longer edge of the specimen (the propagation path

341   was parallel to the stiffener). Such placement of the transducers allowed for avoiding the

342   interference of reflections from edges and from stiffener with an incident wave which is further

343   processed. Indeed, the influence of the additional structural elements should be included in

344   further research. However, because the main aim of the present study is to develop and test the

345   novel procedure of the corrosion degradation level assessment, we have used the favourable

346   configuration of the transducers.

347   The reconstructed dispersion curve allows for assessing the corrosion degradation level
348 along the propagation path. The longer the distance, the greater the monitored area, and the
349 corrosion's thickness variability will be estimated as an equivalent average plate thickness.

350   The newly developed approach was tested in dispersion curve reconstruction on shorter
351 distances not exceeding a few centimetres. The short distance minimises the dispersion effects
352 and allows for a better characterisation of the corroded plate thickness variability as an
353 equivalent average plate thickness. However, in large-scale offshore or ship structures,
354 attaching sensors very close to each other would be inefficient. The distance of 30 cm was
355 chosen to compromise the size of the monitored area of the stiffened plate and the resolution of
356 the corrosion degradation plate surface roughness. Testing of more extended objects is possible
357 with adequate amplifying of the excitation. It is also possible to use a different approach like
358 multiple inputs-multiple outputs and a comprehensive sensor network to increase the monitored
359 area.

360

361 **4   Analysis and results**

362   Wave propagation signals were processed to estimate the group propagation velocity for
363 various frequencies and determine the average corroded plate thickness along the propagation
364 path. The analysis was implemented in a MATLAB environment, and the adopted filtering
365 parameters are summarised in Table 1.

366 Table 1 Parameters of the Gaussian filters

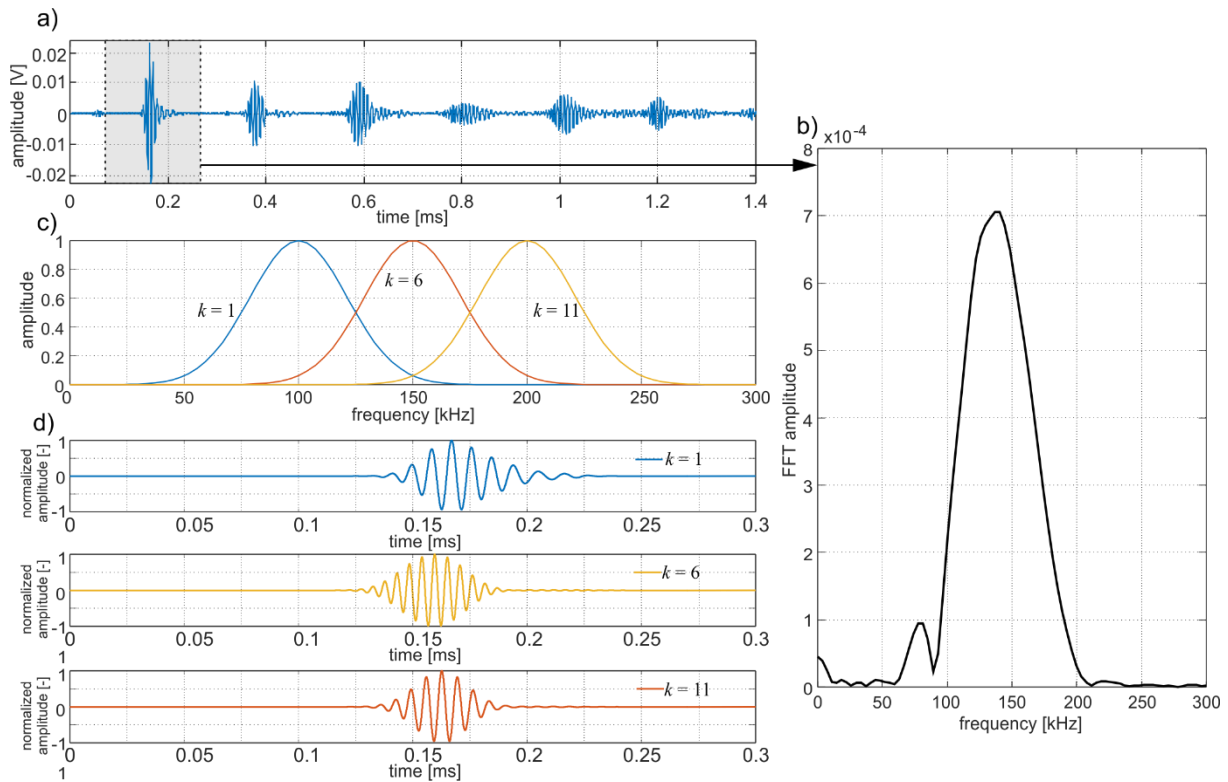| excitation frequency [kHz]	frequency limits [kHz]		filter bandwidth ΔB [kHz]	filters number K [-]
	f_L	f_H		
50	35	65	20	11
100	70	130	40	11
150	100	200	50	11
200	130	260	60	11
250	160	330	60	11

367

16

Figure 9 Signal processing: a) registered time-domain signal, b) Fourier transform of the extracted incident wave, c) filters and d) reconstructed signal after filtering

An exemplary signal captured by sensor S2 registering for the corroded plate (corrosion degradation level 7%) and the excitation frequency of 150 kHz, as well as the intermediate results in the form of a Fourier spectrum, filters, and three signals obtained for k equals to 1, 6 and 11 are presented in Figure 9.

The analysis has been divided into two stages. The dispersion curve has been reconstructed within the first stage based on the ten signals registered for five different frequencies. Thus, in total, ten signals were processed. In the second stage, the dispersion curve has been determined based on only two adjacent signals registered for one frequency.

4.1   *Dispersion curve reconstruction based on several excitation frequencies*

Figure 10 presents the results of reconstructing the dispersion curves for any particular specimens. Experimental outcomes are denoted by red dots, while the solid black line depicts the Lamb dispersion curve characterised by the minimal value of $Y(d)$ (Eqn 10). Despite the experimental group velocity coinciding well with the dispersion curve, the difference in matching the analytical solution is visible, confirming the correctness of the proposed algorithm of dispersion curve reconstruction. The most significant deviation of experimental results from the theoretical curve was obtained for the specimen characterised by the highest corrosion degradation level (Figure 10d), which the more intense wave integration may cause with

17

388 irregularities of the corroded surface, as well as with the most significant deviation of the plate
389 thickness from the average value.
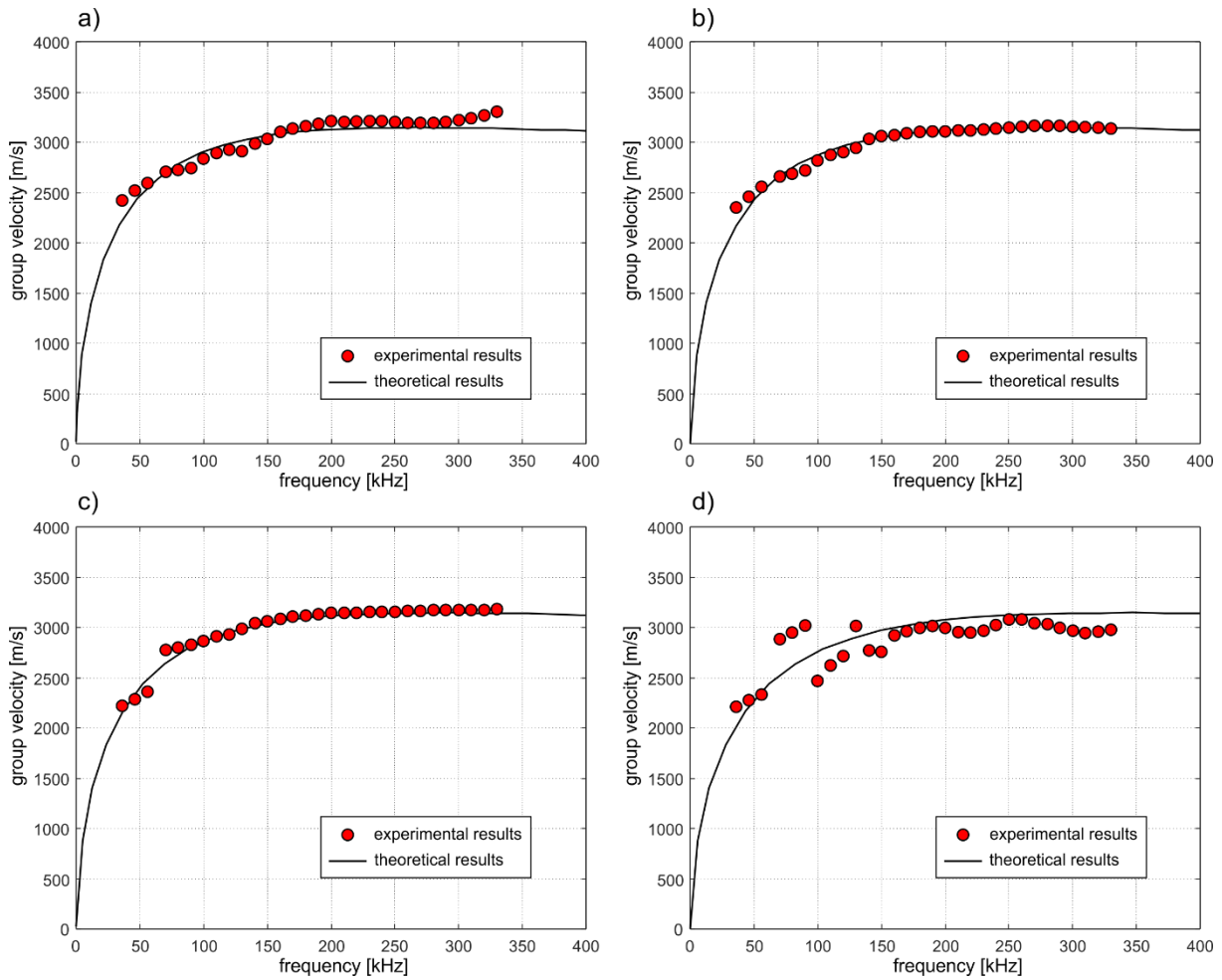
390

391 Figure 10 Reconstruction of dispersion curves for a) specimen #1, b) specimen #2, c) specimen #3 and d)
392 specimen #4

393   The estimated parameters of the analysed corroded plates are summarised in Table 2. The
394 estimated corrosion level C_a has been calculated based on the determined plate thickness from
395 the fitted dispersion curve:

$$C_d = \frac{d_t}{d} \cdot 100\% \ , \qquad (11)$$

396

397 where d is the thickness of the uncorroded plate determined non-destructively, and d_t is the
398 thickness of the corroded plate, where d was estimated as 5.18 mm. Comparing the results for
399 corroded and uncorroded plates, it can be seen that the guided wave propagation approach limits
400 the inaccuracies of determination of propagation velocity caused by the chosen method of the
401 time-of-flight calculation and the influence of deviation of material parameters. On the other
402 hand, the reference signals registered for the original structure are required for such comparison.
403 Still, it can be noticed that the reference measurement does not have to be made on the same
404 structure.

18

405   The estimated corrosion degradation levels differ slightly from the actual one, but a good

406   agreement between the results is observed. The absolute error, which is defined as the difference

407   between the accurate and estimated equivalent average thickness:

408
$$e_a = |d_a - d_t| \qquad (13)$$

409   did not exceed 0.5 mm, which indicates that the plate thickness may be estimated with high

410   accuracy even without reference measurements. The maximum value of the relative error

411   referencing to actual thickness:

412
$$e_r = \frac{e_a}{d_a} \cdot 100\% , \qquad (14)$$

413   is equal to 10.42% and was obtained for specimen #3 but is can be explained by the fact that

414   the general corrosion is not associated with perfect uniform thickness reduction. The higher

415   corrosion level C_d does not exclude that in some regions the thickness reduction is smaller and

416   opposite.

417   Table 2 Average corrosion degradation level of stiffened plates

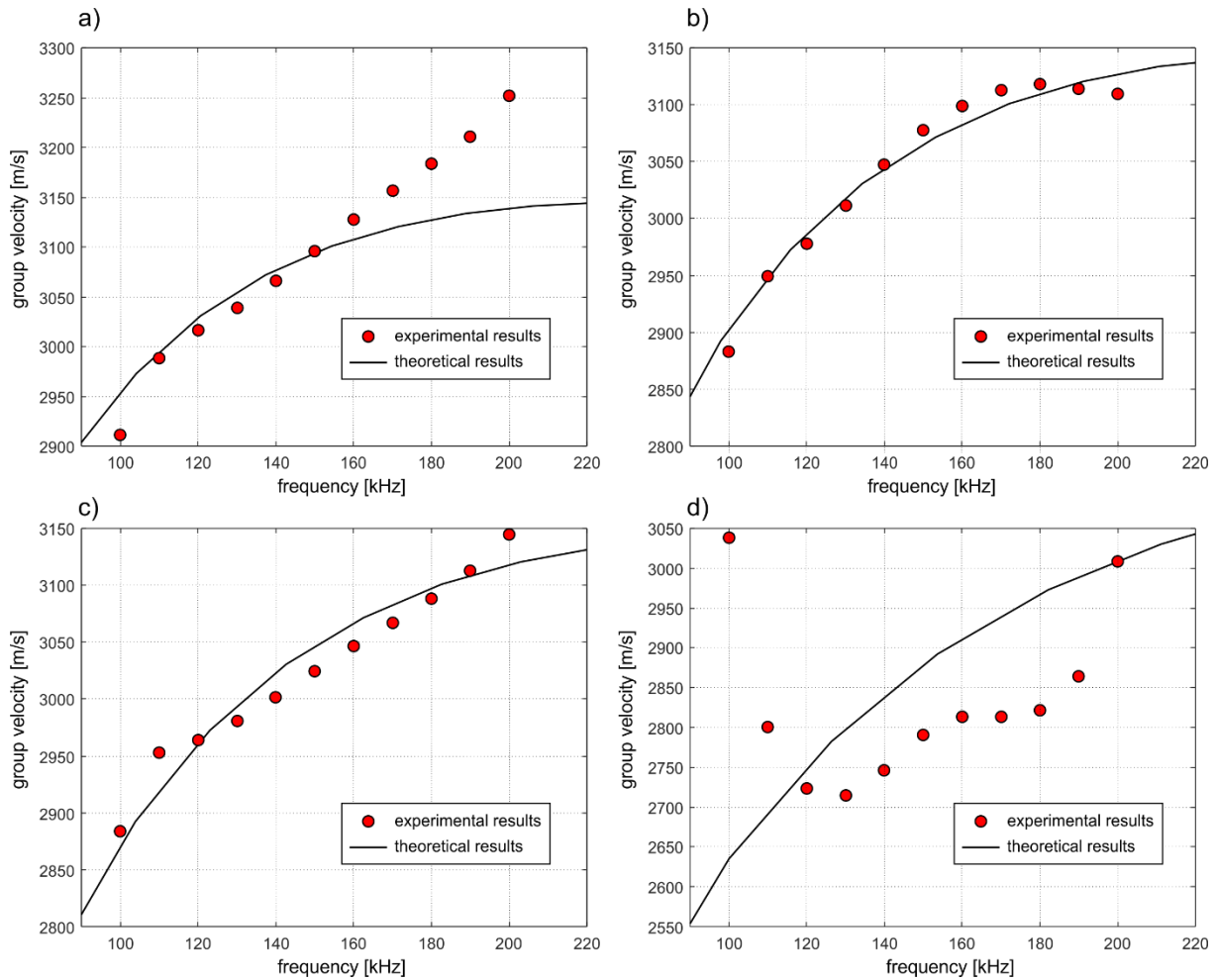| specimen	actual corrosion level C_d [%]	average thickness d_a [mm]	thickness determined by Lamb waves d_t [mm]	estimated corrosion level C_a [%]	absolute error e_a [mm]	relative error e_r [%]
#1	0	5	5.180	0	0.180	2.40
#2	7	4.638	4.890	4.500	0.252	5.43
#3	14	4.320	4.770	6.835	0.450	10.42
#4	21	3.948	4.000	21.875	0.052	1.32

418

419   *4.2   Dispersion curve reconstruction based on one excitation frequency*

420   An attempt of corrosion degradation assessment based on one excitation frequency and

421   only one pair of signals captured at points S1 and S2 were made. The segment of the dispersion

422   curve has been reconstructed based on the measurement made for an excitation frequency of

423   150 kHz. Based on the theoretical solution traced for uncorroded plate (Figure 2), one can

424   conclude that relatively low frequencies (<100 kHz) are highly dispersive, which means that

425   low-frequency change results in a significant alteration in the propagation velocity.

426   Consequently, the shape of the propagating wave packet varies significantly along the

427   propagation path. The potential inaccuracies in measuring the distance between sensors or

428   calculating the flight time result in a substantial over-or underestimation of the propagation

429   velocity. Despite that this frequency range seems to be sensitive to plate thickness changes, the

430   reconstruction of the dispersion curve may be laden with a substantial error.

19

431   In turn, for the high frequencies (>200 kHz), the dispersion curve becomes flat, the
432   velocity for various frequencies is similar, and the shape of the propagating wave packet
433   remains unchanged. Moreover, the higher the frequency, the shorter the wave becomes and thus
434   is much more sensitive to the surface irregularities caused by corrosion degradation. In the
435   signal, additional reflections are registered, which hinders the unambiguous indication and
436   further extraction of incident waves for the analysis. The wave energy is dissipated faster, and
437   the SNR decreases. Moreover, one can see that the higher frequencies become insensitive to
438   the thickness reduction. The plate thickness reduction is associated with an insignificant
439   propagation velocity change. Considering all aspects mentioned above, a "medium" frequency
440   of 150 kHz is used, which is a compromise between dispersion effects, SNR, and sensitivity to
441   corrosion damage.

442   Figure 11 depicts the experimental group velocities and reconstructed dispersion curves,
443   while the corrosion degradation level assessment is summarised in Table 3. The corrosion
444   degradation level assessment accuracy is lower when the curve is traced based on only one
445   measurement. However, still, a good agreement between actual and estimated corrosion
446   degradation levels was noted. In all cases, the corrosion degradation level has been
447   overestimated. However, the absolute error did not exceed 0.8 mm.

448   The most significant deviations of experimental outcomes from the theoretical solution
449   are observed at the ends of the considered frequency range for the highest and the lowest
450   frequency components of the fundamental antisymmetric mode (100 and 200 kHz). The main
451   reason may be the presence of the side lobes, which were not eliminated from the frequency
452   spectrum despite windowing the input signal and subsequent filtering the Fourier spectrum
453   (Lyons, 2011). The same effect was also observed in the previous investigation stage for other
454   frequencies. Still, the averaging of overlapping curve segments at the ends of the frequency
455   range (Figure 4b) reduced the deviations from the theoretical curve.

456
457   Figure 11 Reconstruction of dispersion curves for a) specimen #1, b) specimen #2, c) specimen #3 and d)
458   specimen #4

459   Table 3 Corrosion degradation level of stiffened plates

specimen	actual corrosion level C_d [%]	average thickness d_a [mm]	thickness determined by Lamb waves d_t [mm]	estimated corrosion level C_a [%]	absolute error e_a [mm]	relative error e_r [%]
#1	0	5	5.770	0	0.770	15.40
#2	7	4.638	5.170	10.399	0.532	11.47
#3	14	4.320	4.870	15.598	0.550	12.73
#4	21	3.948	3.290	42.981	0.658	16.67

460   *4.3   Calibration and error mitigation*

461   There are several different sources of inaccuracies where one of the most compelling

462   reasons in the applied approach is the time of the flight. In this study, the time of flight was

463   defined as a difference in the registration time of the peaks of the signal envelopes determined

464   by using the cross-correlation method. However, there are many developed approaches for

465   flight estimation, and the results differ slightly depending on which method was chosen (Xu et

466   al., 2009). Because the thickness was overestimated in most cases, one can conclude a

21

467 systematic error made during the velocity determination. In the considered frequency range, the
468 increase of velocity is related to an increase in the thickness. Thus, possibly the applied method
469 of the time of flight determination based on cross-correlation of the Hilbert transform of
470 adjacent signals resulted in underestimating the registration time.

471   To investigate whether the systematic error of velocity determination influenced the
472 results, the following analysis has been conducted: based on the analytical and experimental
473 dispersion curves obtained for an undamaged plate with a known thickness of $d = 5$ mm., the
474 error has been determined. The velocity overestimation was $\Delta = 19$ m/s. The velocities obtained
475 for other stiffened plates have been reduced by Δ, which means that the obtained curves were
476 just shifted down without changing their shapes, and then the procedure of the corrosion level
477 identification has been applied (Section 2.3). Table 4 contains the results obtained after
478 calibrating the velocity based on an uncorroded plate. It is visible that calibrating the velocity
479 increases the quality of the estimated corrosion degradation level. It is noted, that in most cases,
480 the presented method overestimates the thickness. However, for Specimen #4, the thickness is
481 underestimated. At that stage of development, this does not allow to make some general
482 conclusions regarding that issue and future studies are needed. The error influence may be
483 limited by conducting the measurements for various frequencies and various distances between
484 the transducers.

485 Table 4 Corrosion degradation level of stiffened plates after velocity calibration

specimen	actual corrosion level [%]	corrosion level estimated based on Lamb waves [%]	
		without velocity calibration	with velocity calibration
#1	0	0	0
#2	7	10.399	5.200
#3	14	15.598	9.500
#4	21	42.981	20.00

486

487 *4.4   Discussion*

488   The results presented in the previous section confirm the proposed algorithm's
489 effectiveness in tracing the dispersion curve and identifying the averaged structural degradation
490 level. The main advantage over so far presented ultrasonic methods dedicated to thickness
491 estimation of corroded ship's structural components is the necessity to collect a limited number
492 of signals. The transducers network does not demand a large number of PZT. The actuator
493 triggered the signals was captured by two sensors and one actuator placed on a line. The first
494 sensor should be attached at a short distance from an actuator, which provides a high-amplitude

22

495   incident wave. The spatial distance between the sensors can be adjusted to the structure size,

496   used equipment, and the desired accuracy of identifying the average corroded plate thickness.

497   A significant advantage is that the presented wave-based method does not require

498   collecting the reference data for an uncorroded structure. The measurements of uncorroded

499   plates improve the quality of the results obtained and allow for better corrosion degradation

500   assessment by reducing the influence of systematic errors, but they are not indispensable.

501   The robustness of the novel procedure was examined in two stages. In the first stage, the

502   group velocity dispersion curve has been reconstructed using signals registered for various

503   excitation frequencies. The main advantage of the approach based on the measurement of

504   several frequencies is that the shape of the dispersion curve can be faithfully reconstructed. On

505   the other hand, the number of required signals and, in consequence, the time of analysis is

506   longer. In the second stage, the signals were registered for only one excitation type. The main

507   advantage of reconstructing only one chosen segment of the dispersion curve is the necessity to

508   use only one excitation frequency for all tested specimens. The assessment of the corrosion

509   degradation demands only two signals be captured at the known distance. However, it also

510   demands the appropriate choice of excitation frequency, which is not a trivial issue and requires

511   considering the shape of the dispersion curve determined based on an analytical equation.

512   Despite promising results, the indispensable prerequisite of the further enhancement of

513   the proposed approach demanded before its practical application is the consideration of its

514   limitations. First, the corrosion degradation identification algorithm does not take into account

515   the plate thickness variability. The corrosion degradation level was indirectly averaged by

516   assuming that the thickness is constant along the propagation path. However, the plate thickness

517   variability can be mapped much better by extending the sensors network or taking additional

518   measurements at other points.

519   The irregularities of the corroded surfaces influenced the quality of the results. The

520   disturbance interactions with abnormalities resulting in wave diffractions and conversions lead

521   to incident wave indication and extraction difficulties for further analysis. Though only one

522   antisymmetric wave mode could propagate within the considered frequency range, wave

523   integration with irregular surfaces might also induce low-energy symmetric wave mode.

524   Propagating of multiple wave packets and their interference affects the shape of the incident

525   wave and, in consequence, the characteristics of the frequency spectrum, which led to

526   inaccuracies in time of flight estimation.

527   The discrepancies between theoretical and experimental results can also originate from

528   the assumption about the constant value of elastic modulus and material density; however, the

529   material parameters are also predefined in standard ultrasonic thickness measurement to
530   calculate the velocity of the pressure wave. Thus, further development of the corrosion
531   degradation level identification algorithm may include the impact on material parameters or
532   fluctuations on the dispersion curve shape. The dependence between wave velocity and any
533   parameter in the dispersion Lamb equation is strongly nonlinear, which means that, e.g., the
534   overestimation of elastic modulus may lead to overestimating wave velocity for one excitation
535   frequency and underestimating for other frequencies. It should be noted that the influence of
536   corrosion degradation on material properties was not considered here. The density, Poisson's
537   ratio, and elastic modulus were assumed the same for all analysed stiffened plates.

538   The next element necessary to consider in further studies is the influence of the additional
539   structural elements affecting wave propagation. The problem of the additional reflections can
540   be solved in two different ways. In general, guided wave-based algorithms are usually used for
541   processing the data collected by specially designed SHM systems. In such cases, signals are
542   measured for various states of the investigated specimen and the reference measurements are
543   available for the investigators. Particular reflections can be identified and interpreted and next
544   excluded on the further stages of monitoring and signal processing. The second way to limit the
545   problem of additional reflections from boundaries and stiffeners is the utilization of different
546   transducer types. Recently, a novel type of frequency steerable transducers has been developed.
547   The novel transducer allows sending of the signal only in one chosen direction, which is
548   dependent on the excitation frequency (Baravelli et al., 2013; De Marchi et al., 2016). The main
549   lobe, characterized by high amplitude propagates in one direction while small-amplitude side
550   lobes propagate in other directions. Even if the total elimination of the boundaries reflections
551   is not possible, their amplitudes can be significantly reduced by focusing wave energy only in
552   an interesting direction.

553 **5   Future perspectives**

554   Since the present study mainly focused on the development of the signal processing which
555   can be potentially used in the SHM systems, several aspects were not considered here and
556   should be investigated in future studies, including:

557   • Ships and offshore structures are large in size and complex in geometry. Their
558   diagnostics would require a more complex sensor network. The optimal sensor
559   placement will be considered. The trade-off between the resolution and extent of the
560   sensors network must be considered.

561   • Practical application of the developed approach requires considering the reliability of the
562   proposed method and the influence of inaccuracies on the determined DoD (Falcetelli et

24

563 al., 2021). This should in particular cover further studies regarding higher thicknesses of
564 analysed plates and related uncertainty levels.

565 • Guided waves are widely used for localized damage detection. Therefore, the possibility
566 of building multi-step algorithms for both general uniform and pitting corrosion detection
567 and evaluation must be investigated.

568 ## 6   Conclusions

569 This study conducted theoretical and experimental investigations of guided wave
570 propagation in corroded stiffened plates. The newly developed approach allows for an average
571 corrosion degradation level identification based on the single measurements of the tested
572 stiffened plates.

573 The experimental data acquired for four different stiffened plates varying in degradation
574 level confirmed the correctness of the developed procedure of dispersion curve reconstruction.
575 The corrosion degradation level identification has been made in several different ways: once
576 the dispersion curve has been traced based on several measurements made for various
577 frequencies. At the same time, in the second case, the signals were captured for only one
578 excitation type. It was proved that the corrosion degradation level was better assessed if the
579 measurements involved a wider frequency range. However, regardless of the considered
580 frequency range within the dispersion curve that has been reconstructed, the corrosion
581 degradation level remained slightly underestimated, which indicated the possible systematic
582 error related to the time of flight and, in consequence, with group velocity estimation. Based on
583 the assumption that the initial thickness of the uncorroded stiffened plate is usually known a
584 priori, the value of systematic error has been established and included in further assessing the
585 corrosion deterioration of other stiffened plates. It allowed for a better estimation of the precise
586 degree of corrosion degradation.

587 The highest deviation between experimental measurements and theoretically defined
588 dispersion curve was observed for the most severely corroded stiffened plates. This allows the
589 hypothesis that the presented methodology could determine the average thickness and its
590 variability level. After further development, the proposed method should be applicable in all
591 cases requiring multiple ultrasonic measurements to assess the thickness of steel structural
592 elements.

593

596

25

References

Baravelli E, Senesi M, Ruzzene M, De Marchi L. Fabrication and Characterization of a Wavenumber-Spiral Frequency-Steerable Acoustic Transducer for Source Localization in Plate Structures. IEEE Trans Instrum Meas 2013;62:2197–204. https://doi.org/10.1109/TIM.2013.2255992.

Cao X, Zeng L, Lin J. Generalized scattering matrix method for Lamb wave scattering analysis at cascaded notches. J Vib Control 2021:107754632110377. https://doi.org/10.1177/10775463211037790.

Cegla F, Gajdacsi A. Mitigating the effects of surface morphology changes during ultrasonic wall thickness monitoring. AIP Conf. Proc., 2016, p. 170001. https://doi.org/10.1063/1.4940624.

Ciampa F, Scarselli G, Pickering S, Meo M. Nonlinear elastic wave tomography for the imaging of corrosion damage. Ultrasonics 2015;62:147–55. https://doi.org/10.1016/j.ultras.2015.05.011.

Ding X, Xu C, Deng M, Zhao Y, Bi X, Hu N. Experimental investigation of the surface corrosion damage in plates based on nonlinear Lamb wave methods. NDT E Int 2021;121:102466. https://doi.org/10.1016/j.ndteint.2021.102466.

Draudviliene L, Tumsys O, Mazeika L, Zukauskas E. Estimation of the Lamb wave phase velocity dispersion curves using only two adjacent signals. Compos Struct 2021;258:113174. https://doi.org/10.1016/j.compstruct.2020.113174.

Ervin BL, Kuchma DA, Bernhard JT, Reis H. Monitoring Corrosion of Rebar Embedded in Mortar Using High-Frequency Guided Ultrasonic Waves. J Eng Mech 2009;135:9–19. https://doi.org/10.1061/(ASCE)0733-9399(2009)135:1(9).

Ervin BL, Reis H. Longitudinal guided waves for monitoring corrosion in reinforced mortar. Meas Sci Technol 2008;19:055702. https://doi.org/10.1088/0957-0233/19/5/055702.

Falcetelli F, Yue N, Di Sante R, Zarouchas D. Probability of detection, localization, and sizing: The evolution of reliability metrics in Structural Health Monitoring. Struct Heal Monit 2021:147592172110607. https://doi.org/10.1177/14759217211060780.

Farhidzadeh A, Salamone S. Reference-free corrosion damage diagnosis in steel strands using guided ultrasonic waves. Ultrasonics 2015;57:198–208. https://doi.org/10.1016/j.ultras.2014.11.011.

Flashback history: Tanker Prestige sinking (Video). 2015.

Howard R, Cegla F. Detectability of corrosion damage with circumferential guided waves in reflection and transmission. NDT E Int 2017;91:108–19. https://doi.org/10.1016/j.ndteint.2017.07.004.

Hu M, He J, Zhou C, Shu Z, Yang W. Surface damage detection of steel plate with different depths based on Lamb wave. Measurement 2022;187:110364. https://doi.org/10.1016/j.measurement.2021.110364.

Hua J, Cao X, Yi Y, Lin J. Time-frequency damage index of Broadband Lamb wave for corrosion inspection. J Sound Vib 2020;464:114985. https://doi.org/10.1016/j.jsv.2019.114985.

ISO. Metallic materials - Tensile testing - Part 1: Method of test at room temperature. Int Stand ISO 6892-1 2009.

Lamb H. On waves in an elastic plate. Proc R Soc London Ser A, Contain Pap a Math Phys Character 1917;93:114–28. https://doi.org/10.1098/rspa.1917.0008.

26

633 Li Z, Wang Y, Zheng J, Liu N, Li M, Teng J. Stress measurement for steel slender waveguides based on the
634 nonlinear relation between guided wave group velocity and stress. Measurement 2021;179:109465.
635 https://doi.org/10.1016/j.measurement.2021.109465.

636 Lyons R. Understanding Digital Signal Processing. 3rd ed. Prentice-Hall; 2011.

637 De Marchi L, Testoni N, Marzani A. A New Generation of Frequency Steerable Transducers for Lamb Waves
638 Inspections. 19th World Conf. Non-Destructive Test. (WCNDT 2016), Munich: 2016, p. 1–8.

639 Melchers RE. Development of new applied models for steel corrosion in marine applications including shipping.
640 Ships Offshore Struct 2008;3:135–44. https://doi.org/10.1080/17445300701799851.

641 Moustafa A, Niri ED, Farhidzadeh A, Salamone S. Corrosion monitoring of post-tensioned concrete structures
642 using fractal analysis of guided ultrasonic waves. Struct Control Heal Monit 2014;21:438–48.
643 https://doi.org/10.1002/stc.1586.

644 Panayotova M, Garbatov Y. Corrosion of steels in marine environment, monitoring and standards. Saf. Reliab.
645 Ind. Prod. Syst. Struct., CRC Press; 2010, p. 369–413. https://doi.org/10.1201/b10572-36.

646 Parunov J, Senjanović I, Guedes Soares C. Hull-girder reliability of new generation oil tankers. Mar Struct
647 2007;20:49–70. https://doi.org/10.1016/j.marstruc.2007.03.002.

648 Ping He. Simulation of ultrasound pulse propagation in lossy media obeying a frequency power law. IEEE Trans
649 Ultrason Ferroelectr Freq Control 1998;45:114–25. https://doi.org/10.1109/58.646916.

650 Sharma S, Mukherjee A. Longitudinal Guided Waves for Monitoring Chloride Corrosion in Reinforcing Bars in
651 Concrete. Struct Heal Monit 2010;9:555–67. https://doi.org/10.1177/1475921710365415.

652 Tian Z, Xiao W, Ma Z, Yu L. Dispersion curve regression – assisted wideband local wavenumber analysis for
653 characterizing three-dimensional (3D) profile of hidden corrosion damage. Mech Syst Signal Process
654 2021;150:107347. https://doi.org/10.1016/j.ymssp.2020.107347.

655 Wandowski T, Malinowski P, Ostachowicz WM. Damage detection with concentrated configurations of
656 piezoelectric transducers. Smart Mater Struct 2011;20:025002. https://doi.org/10.1088/0964-1726/20/2/025002.

657 Woloszyk K, Garbatov Y, Kowalski J. Indoor accelerated controlled corrosion degradation test of small- and large-
658 scale specimens. Ocean Eng 2021;241:110039. https://doi.org/10.1016/j.oceaneng.2021.110039.

659 Woloszyk K, Kahsin M, Garbatov Y. Numerical assessment of ultimate strength of severe corroded stiffened
660 plates. Eng Struct 2018;168:346–54. https://doi.org/10.1016/j.engstruct.2018.04.085.

661 Xiao L, Peng J, Zhang J, Ma Y, Cai CS. Comparative assessment of mechanical properties of HPS between
662 electrochemical corrosion and spray corrosion. Constr Build Mater 2020;237:117735.
663 https://doi.org/10.1016/j.conbuildmat.2019.117735.

664 Xu B, Yu L, Giurgiutiu V. Advanced methods for time-of-flight estimation with application to Lamb wave
665 structural health monitoring. Proc. 7th Int. Work. Struct. Heal. Monit., Palo Alto, CA, USA: 2009.

666 Yuan Y, Ji Y, Shah S. Comparison of Two Accelerated Corrosion Techniques for Concrete Structures. ACI Struct
667 J 2007;104:344–7. https://doi.org/10.14359/18624.

668 Zayed A, Garbatov Y, Guedes Soares C. Corrosion degradation of ship hull steel plates accounting for local

669 environmental conditions. Ocean Eng 2018;163:299–306. https://doi.org/10.1016/j.oceaneng.2018.05.047.

670 Zayed A, Garbatov Y, Guedes Soares C. Non-destructive Corrosion Inspection Modeling of Tanker Structures.
671 Vol. 2 Struct. Saf. Reliab., ASMEDC; 2008, p. 465–76. https://doi.org/10.1115/OMAE2008-57500.

672 Zima B. Determination of stepped plate thickness distribution using guided waves and compressed sensing
673 approach. Measurement 2022;196:111221. https://doi.org/10.1016/j.measurement.2022.111221.

674 Zima B. Damage detection in plates based on Lamb wavefront shape reconstruction. Measurement
675 2021;177:109206. https://doi.org/10.1016/j.measurement.2021.109206.

676 Zima B, Rucka M. Guided wave propagation for assessment of adhesive bonding between steel and concrete.
677 Procedia Eng 2017;199:2300–5. https://doi.org/10.1016/j.proeng.2017.09.189.

678 Zima B, Woloszyk K, Garbatov Y. Corrosion degradation monitoring of ship stiffened plates using guided wave
679 phase velocity and constrained convex optimization method. Ocean Eng 2022;253.

680